Journal of Inorganic Biochemistry 106 (2012) 143–150

Contents lists available at SciVerse ScienceDirect

Journal of Inorganic Biochemistry

journal homepage: www.elsevier.com/locate/jinorgbio

Simultaneous true, gated, and coupled electron-transfer reactions and energetics of protein rearrangement

Tijana Ž. Grove [a], G. Matthias Ullmann [b], Nenad M. Kostić [c,*]

[a] Department of Chemistry, Iowa State University, Ames, Iowa 50011-3111, United States
[b] Structural Biology/Bioinformatics, University of Bayreuth, Universitätsstr. 30, BGI 95447 Bayreuth, Germany
[c] Department of Chemistry, Texas A&M University at Commerce, Commerce, Texas 75429-3011, United States

ARTICLE INFO

Article history:
Received 11 May 2011
Received in revised form 6 September 2011
Accepted 9 September 2011
Available online 17 September 2011

Keywords:
Electron transfer
Metalloproteins
Kinetics and mechanisms
Oxidoreduction reactions
Brownian dynamics

ABSTRACT

Cytochromes c_6 and *f* react by three et mechanisms under similar conditions. We report temperature and viscosity effects on the protein docking and kinetics of ^{3}Zncyt c_6 + cyt *f*(III) → Zncyt c_6^+ + cyt *f*(II). At 0.5–40.0 °C, this reaction occurs within the persistent (associated) diprotein complex with the rate constant k^{pr} and within the transient (collision) complex with the rate constant k^{tr}. The viscosity independence of k^{pr}, the donor-acceptor coupling $H_{ab} = (0.5 \pm 0.1)\,cm^{-1}$, and reorganizational energy $\lambda = (2.14 \pm 0.02)$ eV indicate *true* et within the persistent complex. The viscosity dependence of k^{tr} and a break at 30 °C in the Eyring plot for k^{tr} reveal mechanisms within the transient complex that are reversibly switched by temperature change. Kramers protein friction parameters differ much for the reactions below ($\sigma = 0.3 \pm 0.1$, $\delta = 0.85 \pm 0.07$) and above ($\sigma = 4.0 \pm 0.9$, $\delta = 0.40 \pm 0.06$) 30 °C. The transient complex(es) undergo(es) *coupled* et below ca. 30 °C and *gated* et above ca. 30 °C. Brownian dynamics simulations reveal two broad, dynamic ensembles of configurations "bridged" by few intermediate configurations through which the interconversion presumably occurs.

1. Introduction

Long-range interprotein electron transfer (et) is essential for the controlled flow of the electrons in biological energy transduction [1,2]. Biological processes can be properly understood only if protein interactions and reactions are understood on the molecular level [3–6]. Origins of biochemical specificity probably lie in dynamics of intermolecular interactions. Successful design of these interactions requires understanding of the mechanisms of docking and rearrangement. Despite vigorous and multidisciplinary current research, mechanisms of electron-transfer reactions of metalloproteins are only partially understood [7]. It is widely accepted that the same pair of redox proteins may form multiple complexes that may undergo essentially the same intracomplex electron-transfer reaction at different rates [5,6]. A number of protein complexes undergo dynamic fluctuations in configuration, but little is known about energetic contribution of the intracomplex rearrangement to the overall reaction mechanism [4,8–11].

The overall oxidoreduction reaction in Eq. (1) involves protein association, rearrangement (equilibrium constant) of the initial configuration(s) (subscript i) into the reactive configuration(s) (subscript r), and electron transfer. The rearrangement and electron-transfer steps are differently combined in true, gated, and coupled

$$A_{ox} + B_{red} \underset{k_{off}}{\overset{k_{on}}{\rightleftarrows}} [A_{ox}{-}B_{red}]_i \underset{k_{-r}}{\overset{k_r}{\rightleftarrows}} [A_{ox}{-}B_{red}]_r \xrightarrow{k_{et}} [A_{red}{-}B_{ox}] \quad (1)$$

kinetic mechanisms [7,12], which are different special cases of the molecular mechanism in Eq. (1). For brevity, and following common practice, we will refer to these cases as "mechanisms". In *true*-electron-transfer mechanism, the rate-limiting step is electron transfer ($k_{et} < k_r$), and the apparent rate constant is simply k_{et}. Reorganizational energy for the electron-transfer step, λ, can be determined by fitting of kinetic results to Marcus theory. In *gated* mechanism the rate-limiting step is the rearrangement ($k_{et} > k_r$); although electron transfer is experimentally monitored, the apparent rate constant is k_r. Now, attempts at fitting to Marcus theory are thwarted by the seeming dependence of the observed reorganizational energy λ on the free energy of rearrangement, ΔG_r. In *coupled* mechanism ET is the slow step ($k_{et} < k_r$). The faster but thermodynamically unfavorable ($K_r < 1$) rearrangement affects the apparent rate constant, which is the product $K_r \cdot k_{et}$. Fitting to Marcus theory yields a composite λ having contributions from both electron-transfer and rearrangement steps [7,12].

True and gated oxidoreduction reactions between metalloproteins are known, but coupled reactions are still rare and are often conflated with gated reactions. These three mechanisms have been elegantly diagnosed, but in studies with different proteins [11,13–19]. It is

* Corresponding author.
E-mail address: Nen.M.Kos@gmail.com (N.M. Kostić).

0162-0134/$ – see front matter © 2011 Elsevier Inc. All rights reserved.
doi:10.1016/j.jinorgbio.2011.09.017

therefore unclear whether the diversity in reactivity comes from different proteins or from different dynamics of protein interactions.

To reach a unified view of protein reactivity, the three mechanisms need to be compared for the same reactants. This is the first report of all three mechanisms occurring with the same protein pair. Cytochrome c_6 and cytochrome *f* from *Chlamydomonas reinhardtii* associate mostly by hydrophobic interaction [11]. We report that different mechanisms can occur in the same system and can be switched on and off by changing temperature. We estimate the rate constants k_r and k_{-r}, the equilibrium constant K_r, and the activation barrier $\Delta G_r^{\neq}$ for the protein rearrangement required for electron transfer.

$$^3\text{Zncyt}c_6 + \text{cyt}f(\text{III}) \rightarrow \text{Zncyt}c_6^{+} + \text{cyt}f(\text{II}). \quad (2)$$

Although the photoinduced reaction in Eq. (2) is not strictly biological, it allows the study of dynamics because the high rate of the electron-transfer step renders the slower rearrangement step detectable. The replacement of the buried metal ion and porphyrin excitation to a triplet state does not affect the cytochrome c_6 surface, docking with cytochrome *f*, and dynamics and energetics of the protein complex [9,20]. Conveniently, the photochemical method does not require external redox agents in solution to initiate the overall reaction. Since temperature and viscosity change would affect both this initial reaction and the subsequent processes of interest, the interpretation of results would be ambiguous. When the interprotein oxidoreduction is triggered by photons, variation in solution conditions will affect only the reaction of interest.

Because both reactants are heme proteins, whose absorption spectra overlap, it would be very difficult accurately to follow spectroscopically the simultaneous oxidation of one heme group and reduction of the other [21]. Replacement of iron(II) ion in cytochrome c_6 with zinc(II) ion further eliminates complications, because the triplet excited state, a reactant, and the cation radical, a product, can readily be monitored at different wavelengths.

2. Materials and methods

2.1. Chemicals and buffers

Distilled water was demineralized to a resistivity greater than 17 MΩ cm by a Barnstead Nanopure II apparatus. Chromatographic resins and gels were purchased from Sigma Chemical Co; hydrogen fluoride, from Matheson Gas Product Inc; nitrogen and ultrapure argon, from Air Products Co.; all other chemicals, from Fisher Chemical Co. All buffers were prepared from the solid salts $NaH_2PO_4 \cdot H_2O$ and $Na_2HPO_4 \cdot 7H_2O$, and had pH of 7.00 ± 0.05 and ionic strength of 10.0 mM.

2.2. Proteins

Cytochrome *f* from *C. reinhardtii,* expressed in *E. coli*, was isolated and purified as described previously [22]. Cytochrome c_6 from *C. reinhardtii* was isolated and purified by the published method [23]. Iron was removed, and the free-base protein was fully reconstituted with zinc(II) ions, by a modification of the standard procedure [24]. Zinc cytochrome c_6 was always kept in the dark. Concentrations of the two proteins were determined from their UV–vis spectra, on the basis of known absorptivities: cytochrome *f*(II), $\Delta\varepsilon_{552} = 26$ - $mM^{-1}\,cm^{-1}$, cytochrome c_6(II), $\Delta\varepsilon_{552} = 20\ mM^{-1}\,cm^{-1}$, and zinc cytochrome c_6, $\Delta\varepsilon_{421} = (2.3 \pm 0.1) \times 10^5\ M^{-1}\,cm^{-1}$ [11]. All proteins were stored in liquid nitrogen. Before each series of experiments, the buffer in protein stock solutions was replaced by the working buffer using so-called ultrafree-4 centrifugal filter, obtained from Millipore Co.

2.3. Laser flash photolysis

Experiments were performed [11] with the second harmonic (at 532 nm) of a Q-switched Nd-YAG laser, which delivered 3.5 ns pulses. The laser output was calibrated with a Scientech H410D power meter. The probe beam from a 250-W QTH lamp passed through a 10-nm interference filter, the sample cell, and another such filter before entering a photodiode detector. Argon was passed first through water and then through the buffer solution. The required volume of buffer was deaerated in a 10-mm cuvette for at least 30 min before proteins were added. Concentration of cytochrome *f*(III) was 3 μM, and that of zinc cytochrome c_6 was 1 μM. Decay of the triplet state was monitored at 460 nm, where the transient absorbance has its maximum. The concentration of the triplet, ^{3}Zncyt c_6, depended on the intensity of the laser pulse and was approximately 0.1 μM. Therefore an approximately 30-fold molar excess of cytochrome *f*(III) over the triplet was maintained, for pseudo-first-order kinetics. Formation and disappearance of the cation radical, Zncyt c_6^+, were monitored at 675 nm, where the difference between the absorbances of this species and the triplet is greatest. To enhance signal-to-noise ratio, at least 50 shots were collected and averaged each time.

2.4. Reaction conditions

As Fig. S1 in the supplement shows, these two proteins do become fully associated. The kinetic effects of viscosity were studied in the sodium phosphate buffer having pH 7.0 and ionic strength of 10 mM. Glycerol was added incrementally to the solution containing zinc cytochrome c_6 and cytochrome *f*(III), and the buffer conditions are identical to those in our previous study [11]. Because viscosity depends on temperature, these additions were made at each temperature anew, for precise control. The viscosity of the solution was determined from the tables in CRC Handbook of Chemistry and Physics, as before [9]. Solutions were gently deaerated for 10 min after each addition of glycerol. Temperature in the range from 0.5 to 40.0 °C was kept with a 30-L circulating bath Forma Scientific CH/P 2067. The actual temperature in the cell was calibrated with an Omega HH-22 digital thermometer and was known with precision of ± 0.1 °C.

2.5. Fittings of the kinetic data

The rate constants for the reaction in Eq. (2) were obtained by well-established analysis of the changes of absorbance at 460 and 675 nm with time. Typical traces are shown in Fig. S2 in the supplement. The former change corresponds to the decay of ^{3}Zncyt c_6 and is a sum of several exponential terms (Eq. (3)). The latter change is caused by both the triplet and the cation radical and is described by Eqs. (4)–(7) [11]. Contribution of the triplet to the absorbance change at 675 nm is given by Eq. (5), in which a_t is the instantaneous absorbance after the laser flash. The contribution of cation radical is fitted with Eq. (7).

$$\Delta A_{460} = \sum_i a_i \exp(-k_i t) + b \quad (3)$$

$$\Delta A_{675} = \Delta A_{\text{triplet}} + \Delta A_{\text{cation}} \quad (4)$$

$$\Delta A_{\text{triplet}} = a_t \left[\sum_i f_i \exp(-k_i t) \right] \quad (5)$$

$$f_i = a_i / \left(a_{\text{pr}} + a_{\text{tr}} \right) i = \text{pr}, \text{tr} \quad (6)$$

$$\Delta A_{\text{cation}} = a_c \left[\exp - \left(k_{fall} t \right) - \exp(-k_{rise} t) \right]. \quad (7)$$

Kinetic results were analyzed with the SigmaPlot v.5.0, from SPSS Inc. The error margins for rate constants, obtained from the fitting of the transient-absorbance changes, may vary in different sets of experiments. In all experiments, however, the margins include two standard deviations, i.e., they correspond to the confidence limit of 95%. This conservative setting

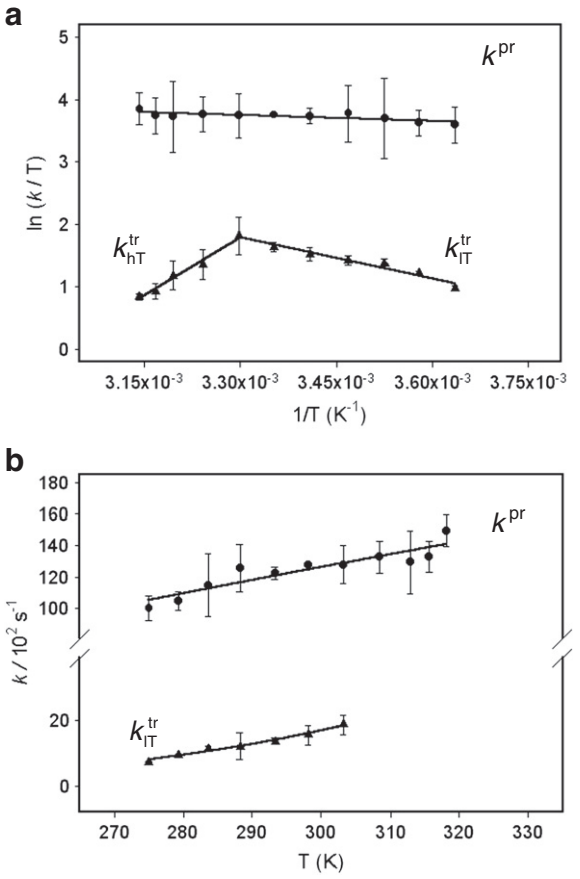

Fig. 1. Temperature dependence of the rate constants k^{pr} and the apparent rate constant k^{tr} in the sodium phosphate buffer at pH 7.0 and ionic strength of 10 mM. The smallest error bars are invisible. The fitting parameters are given in Table 1. (a) The lines are fittings to Eq. (11). Data below and above the break at 30 °C were fitted separately, as k_{IT}^{tr}(subscript for "low temperature") and k_{hT}^{tr}(subscript for "high temperature"). (b) The fittings to Eqs. (13) and (14) overlap.

of error margins is a precaution against overinterpretation of small differences.

2.6. Brownian dynamics simulations

The association of cytochrome *f* and cytochrome c_6 at ionic strengths of 10 and 200 mM was simulated with the program Macrodox.(*24*) The theoretical basis of these simulations is described in detail elsewhere [25,26]. Cytochrome c_6 moved in the electrostatic potential of cytochrome *f*. The energy was calculated by multiplying the charges of cytochrome c_6 with the electrostatic potential that arises from cytochrome *f*. The electrostatic potential in these simulations is described by the Poisson–Boltzmann equation [27]. A complex was considered to be formed when its energy was less than -7 k_BT. This cut-off was chosen to get a reasonable number of docked configurations. In Fig. 3a, the probability of a docked configuration occurring in the most-populated energy-distance bin was set to unity, and populations of other bins were normalized to this value.

3. Results and discussion

3.1. Mechanism of photoinduced oxidoreduction reaction between zinc cytochrome c_6 and cytochrome f(III)

Laser flash produces the triplet state of zinc porphyrin, ^{3}Zncyt c_6, which is a strong reducing agent. The high driving force (1.2 V) makes electron transfer from ^{3}Zncyt c_6 to cyt *f*(III) fast, so that underlying dynamic processes become observable. In the absence of a quencher, natural decay of the triplet state of the porphyrin to its ground state is monoexponential (Eq. (8)). The rate constant k_{nd} for this natural decay is $100\pm10\ s^{-1}$ in the temperature range from 0.5 to 40.0 °C in the phosphate buffer at pH 7.00 and is independent of protein concentration in the interval from 1.0 to 10 μM and ionic strength in the interval from 2.5 to 700 mM.

$$\Delta A_{460} = a_{nd}\exp(-k_{nd}t) + b. \tag{8}$$

In the presence of cytochrome *f*(III), the decay of the triplet accelerates and is well described with two exponentials (Eq. (9)).

$$\Delta A_{460} = a_1\exp(-k^{pr}t) + a_2\exp\left(-k^{tr}t\right) + b. \tag{9}$$

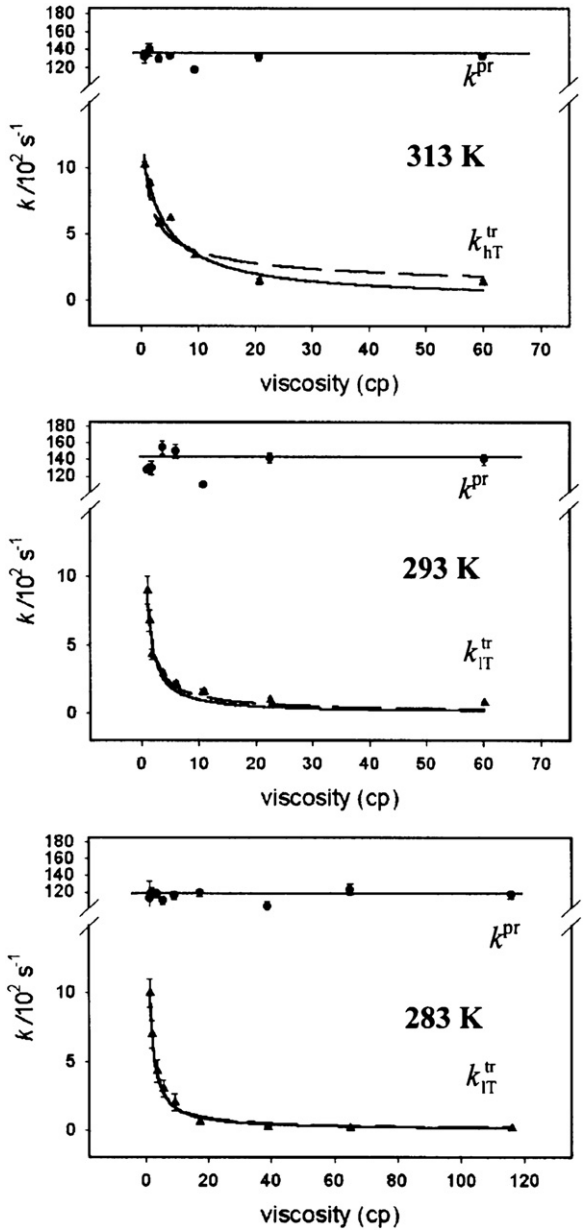

Fig. 2. Viscosity independence of the rate constants k^{pr} and viscosity dependence of the apparent rate constants k_{IT}^{tr}(subscript for "low temperature") and k_{hT}^{tr}(subscript for "high temperature") in the sodium phosphate buffer at pH 7.0 and ionic strength of 10 mM. The smallest error bars are invisible. Solid lines are fittings to Eq. (15); dashed, to Eq. (16). Fitting parameters are shown in Table 2.

Zncyt c_6 exists in solution free and bound, i.e., unassociated and associated with cyt *f*(III). Both forms of the protein become excited into ^{3}Zncyt c_6, and both are then oxidatively quenched by cyt *f*(III); hence biphasic kinetics. The bound triplet undergoes a unimolecular electron-transfer reaction involving the persistent complex (right-hand side of Scheme 1). The free triplet and cyt *f*(III) form transient complex(es) that rearrange (s) into redox-active configuration(s) (left-hand side of Scheme 1). The observed rate constant k^{pr} (persistent pathway), for the faster phase, is independent of cyt *f*(III) concentration, whereas the apparent rate constant k^{tr} (transient pathway), for the slower phase, increases and then levels off at relatively high cytochrome *f*(III) concentrations [11]. To avoid complications arising from dependence of k^{tr} on cytochrome *f*(III) concentration, protein concentrations were adjusted so that cytochrome *f*(III) was always present in excess over zinc cytochrome c_6. Consequently, the maximal value of k^{tr} is achieved. The unimolecular intracomplex rate constants for the persistent (k^{pr}) and transient (k^{tr}) complexes in Scheme 1 differ as much as thirteenfold, $k^{pr} = (1.2 \pm 0.1) \times 10^4\ s^{-1}$, and $k^{tr} = (9 \pm 4) \times 10^2\ s^{-1}$ in the phosphate buffer having pH 7.00 and ionic strength of 10 mM, at room temperature [11].

The rate constants for the appearance and disappearance of the redox intermediate, cation radical, are independent of the cytochrome *f*(III) concentration. The increase in the absorbance at 675 nm is due to the back reaction (Eq. (10)), and its decrease is due to the forward reaction of interest (Eq. (2)) [9]. The appearance and disappearance of cation radical were monitored throughout the temperature range.

$$\text{Zncyt}c_6^{+} + \text{cyt}f(\text{II}) \rightarrow \text{Zncyt}c_6 + \text{cyt}f(\text{III}) \tag{10}$$

3.2. Kinetic effects of temperature

Classical transition-state theory (Eqs. (11) and (12)) assumes that when activation energy is achieved the reaction occurs with a probability of approximately one. In that case Eq. (11) shows the enthalpy and the entropy of activation corresponding to the transition state. Protein oxidoreduction reactions are nonadiabatic, and Marcus theory (Eqs. (13) and (14)) takes this into account.

$$k = \frac{k_B T}{h} \exp\frac{\Delta S^{\neq}}{R} \exp\frac{-\Delta H^{\neq}}{RT} \tag{11}$$

$$\Delta G^{\neq} = \Delta H^{\neq} - T\Delta S^{\neq} \tag{12}$$

$$k = \frac{4\pi^2 H_{AB}}{h(4\pi\lambda RT)^{1/2}} \exp\left[\frac{-\left(\Delta G^0 + \lambda\right)^2}{4\lambda RT}\right] \tag{13}$$

$$k = k_0 \exp[-\beta(r - r_0)] \exp\left[\frac{-\left(\Delta G^0 + \lambda\right)^2}{4\pi RT}\right]. \tag{14}$$

In these equations λ is the reorganizational energy, H_{AB} is the donor-acceptor electronic coupling, h is the Planck constant, T is the temperature, R is the gas constant, k_0 is the characteristic nuclear frequency ($10^{13}\ s^{-1}$), r is the donor-acceptor distance, r_0 is the contact distance (3 Å), and the β (set at $1\ Å^{-1}$) describes the intervening medium. ΔG^0 is determined from the ΔE_m value for the reaction (1.2 V).

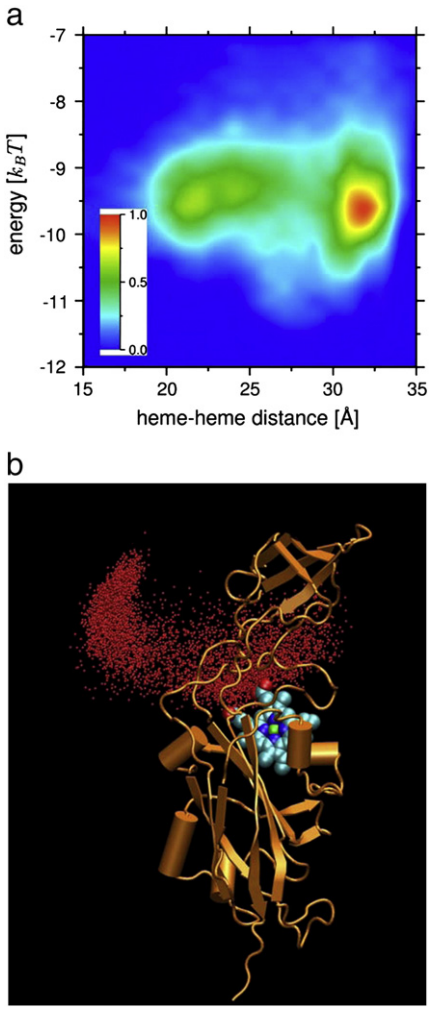

Fig. 3. Results of Brownian-dynamics simulation of cytochrome c_6 and cytochrome *f* at ionic strength of 10 mM. One million trajectories gave about 110,000 diprotein configurations having association energy of −7 k_BT or lower. (a) Color-coded probability of association as a function of the protein interaction energy and the shortest heme–heme distance. (b) Cytochrome *f* and centers of mass of 5000 cytochrome c_6 molecules randomly chosen from 110,000.

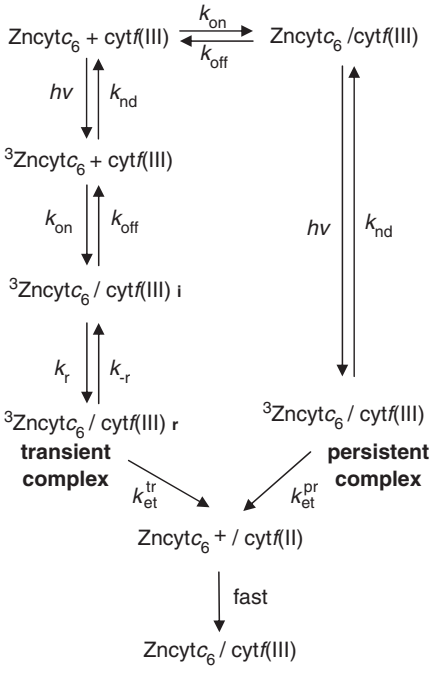

Scheme S1. Kinetic mechanism.

Biphasic kinetics and detectable Zncytc_6^+ in the entire interval covered, from 0.5 to 40.0 °C, show that the two-path mechanism in Scheme 1 operates throughout. We fitted temperature dependence of k^{pr} and k^{tr} to Eq. (11) to determine enthalpy ($\Delta H^{\neq}$) and entropy ($\Delta S^{\neq}$) of activation, and then obtained free energy of activation ($\Delta G^{\neq}$) with Eq. (12). Since the interpretation of activation parameters for nonadiabatic reactions is ambiguous, $\Delta H^{\neq}$, $\Delta S^{\neq}$, and $\Delta G^{\neq}$ are given only for comparison of the processes within persistent and transient complexes. Unexpectedly but consistently, inspection of Fig. 1a and comparison of the values for $\Delta H^{\neq}$, $\Delta S^{\neq}$, and $\Delta G^{\neq}$ (Table 1) for the reactions within persistent and transient complexes point at three different intracomplex reactions: that within the persistent complex and those within the transient complex(es) above and below ca. 30 °C. The break in Fig. 1a suggests a change of mechanism for the transient complex. This change is reversible by heating and cooling and probably occurs gradually around 30 °C. To our knowledge, such a "broken" Eyring plot has not been reported before for protein oxidoreduction reactions.

Temperature effects on the reaction in Eq. (2) clearly show the existence of three mechanisms. Analysis of these effects in terms of Marcus theory can provisionally classify the mechanisms as true, coupled, or gated. Bearing in mind that this method is inconclusive, we consider Fig. 1b and the bottom three rows in Table 1. A λ value between ca. 0.7 and ca. 2.3 eV and H_{AB}<80 cm^{-1} is symptomatic of true-electron-transfer mechanism [7], and we cautiously assign it to the reaction within the persistent complex. A λ value exceeding ca. 2.3 eV is symptomatic of gated mechanism if accompanied by H_{AB}>80 cm^{-1} and of a coupled mechanism if accompanied by H_{AB}<80 cm^{-1}. Consistent fittings of k_{1T}^{tr} to Eqs. (13) and (14) gave the latter combination of results, and we tentatively assign the coupled mechanism to the reaction within the transient complex below ca. 30 °C. Marcus theory does not apply to k_{hT}^{tr} because this rate constant reproducibly decreases as temperature increases. We will discuss this interesting case below.

Brownian dynamics simulation of the association of cytochrome c_6 and cytochrome *f* yielded many complexes having interaction energies lower than −7 kT in which the distance between the redox centers falls between 12 and 32 Å. Fittings of k^{pr} and k_{1T}^{tr} to Eq. (14) also gave edge-to-edge distance between electron donor and electron acceptor well within this range. Since Marcus theory seems to apply to these two processes, we cautiously confirm that in them electron transfer is involved in the rate-limiting step. To further explore the three detected processes, we varied solution viscosity.

3.3. Kinetic effects of viscosity

In previous studies in our laboratory, variation of solution viscosity was introduced as an experimental method for detecting structural rearrangement of protein complexes. Nonbinding and conformationally noninvasive viscogens increase molecular friction, impede protein motion, and slow down protein rearrangement, without affecting the rate constant for the electron-transfer step and equilibrium constants [9,11,14,17–19,28–30]. Indeed, noneffect of glycerol on association is evident in supplemental Fig. S3.

The rate constant k^{pr} does not depend on viscosity, but the apparent rate constant k^{tr} does. The viscosity dependence of the rate constants k_{1T}^{tr} and k_{hT}^{tr}, shown in Fig. 2, was fitted to empirical Eqs. (15) and (16), in which η is solvent viscosity, $\Delta G^{\neq}$ is the free energy of activation for the rearrangement, and σ and δ are parameters related to the protein friction. Eq. (15) is based on a modified form of Kramers's theory that recognizes importance of Brownian fluctuation in overcoming energy barrier for a process and assumes the existence of more that two possible configurations. Eq. (16) reduces to Kramers's equation when δ = 1. Both equations have been used to detect configurational rearrangement of protein–protein and peptide–protein complexes. The fitting results are listed in Table 2.

$$k = \frac{k_B T}{h}\frac{1+\eta}{\sigma+\eta}\exp\left[\frac{-\Delta G_{\sigma}^{\neq}}{RT}\right] \quad (15)$$

$$k = \frac{k_B T}{h}\eta^{-\delta}\exp\left[\frac{-\Delta G_{\delta}^{\neq}}{RT}\right]. \quad (16)$$

The markedly different values above and below 30 °C in Table 2 confirm that temperature change effects a mechanism change in the transient complex. Because σ and δ values depend on the protein surfaces accessible to the solvent, and exposed surfaces in turn depend on buried surfaces, the interface in the transient complex seems to change around 30 °C. Viscosity effects confirmed that the same two proteins react by three different mechanisms, which will be discussed separately below.

3.4. Reaction within the persistent complex

The small H_{AB} and reasonable λ values in Table 1 and viscosity independence of k^{pr} consistently indicate that the persistent complex undergoes a nonadiabatic, true electron-transfer reaction [7]. The negative entropy of −15 J K^{-1} mol^{-1} in Table 1 suggests that considerable "tightening" of the complex is involved in its activation for the electron-transfer step [17]. The persistent complex evidently is dynamic. We surmise that only some of its configurations are redox-active, and that configurational fluctuation probably is too fast to affect the electron-transfer step, which then is rate-limiting. It is tempting to attribute the aforementioned Marcus parameters to the redox-active configurations of the persistent complex, but direct evidence is unobtainable.

3.5. Reactions within the transient complex

Since photoinduced reactions have relatively high driving force, one may ask whether with increasing temperature $-\Delta G^0$ becomes larger than λ [31]. For the photoinduced reaction in Eq. (2) to switch from normal to inverted region, its driving force ($-\Delta G^0$) would have to increase from 1.2 eV to at least 2.0 eV, the magnitude of λ. The change of 0.8 eV or more over a temperature interval of only 40 °C

Table 1
Temperature dependence of the rate constant k^{pr} and k^{tr} (Scheme S1) fitted to Eyring (Eqs. (11) and (12)) and Marcus (Eqs. (13) and (14)) theories.

Fitted parameter (unit)	Persistent complex, k^{pr}	Transient complex<30 °C, k_{1T}^{tr}	Transient complex>30 °C, k_{hT}^{tr}	Fitting equation
$\Delta H^{\neq}$ (kJ/mol)	2.6 ± 0.1	18.4 ± 0.4	−52 ± 1	11
$\Delta S^{\neq}$ (J K^{-1} mol^{-1})	−158 ± 5	−122 ± 10	−350 ± 30	11
$\Delta G^{\neq}$ (kJ/mol)[a]	49 ± 4	54 ± 6	57 ± 6	12
H_{AB} (cm^{-1})	0.5 ± 0.1	4.9 ± 0.5	n. d.[b]	13
λ (eV)	2.1 ± 0.1	3.1 ± 0.2	n. d.[b]	13
λ (eV)	1.9 ± 0.1	3.0 ± 0.2	n. d.[b]	14

[a] Room temperature.
[b] Fitting to Marcus theory is unjustifiable.

Table 2
Friction parameters and activation parameters for the reaction within transient complex.

T (K)	Eq. (15)		Eq. (16)	
	σ	ΔG_{σ} (kJ/mol)	δ	ΔG_{δ} (kJ/mol)
313, k_{hT}^{tr}	4.0 ± 0.9	59.8 ± 0.2	0.40 ± 0.06	59.0 ± 0.4
293, k_{1T}^{tr}	0.2 ± 0.1	56.0 ± 0.2	0.82 ± 0.09	55.3 ± 0.2
283, k_{1T}^{tr}	0.3 ± 0.2	53.2 ± 0.2	0.89 ± 0.05	52.5 ± 0.2

is improbable; even a much smaller change is unlikely. Interplay between the complex rearrangement and electron transfer is a much more reasonable cause of the temperature dependence of k^{tr}.

Both $\Delta H^{\neq}$ and $\Delta S^{\neq}$ in Table 1 markedly change as temperature crosses the 30 °C mark. Moreover, these two changes compensate each other and are invisible in the composite $\Delta G^{\neq}$ values. That $\Delta S^{\neq}$ is negative for both branches of the "broken" Eyring plot in Fig. 1 suggests that structural "tightening" of the complex, presumably to improve the donor-acceptor coupling, is required for electron transfer in all cases [17]. That the $\Delta S^{\neq}$ values are very different for the two branches of the plot confirms that different mechanisms operate in the two temperature intervals. Next, we will discuss these two intervals separately.

3.6. Gated electron-transfer reaction, above ca. 30 °C

The high-temperature branch of the broken plot in Fig. 1a shows that the rate constant decreases with increasing temperature. As discussed above, this rules out interprotein electron transfer and requires discussion of k_{hT}^{tr} in terms of non-redox processes in Eq. (1). Indeed, viscosity dependence of k_{hT}^{tr} (Fig. 2) is diagnostic of structural rearrangement.

The negative $\Delta H^{\neq}$ value in Table 1 requires comment. Negative activation enthalpies are rare, and we think unknown for metalloprotein reactions. Two general explanations exist [32,33]. In one, the reaction mechanism may involve an enthalpically favorable and fast preequilibrium step [32]. In Eq. (1) this would be the rearrangement, defined by K_r. The "pre-equilibrium" condition would require $k_{et} \ll k_{-r}$. Because k^{pr} in Scheme 1 represents true et, k^{pr} applies to the electron-transfer step in any mechanism involving this particular protein pair. We justifiably substitute k^{pr} for k_{et} in Eq. (1), to obtain $k^{pr} = 1\times10^4\ s^{-1} = k_{et}$. Hence the lower limit was $k_{-r} > 1\times10^4\ s^{-1}$ for this gated mechanism. In another explanation, negative $\Delta H^{\neq}$ with positive $\Delta G^{\neq}$, as in our case, suggests that the transition state resembles the products [33]. Indeed, in structural interconversion of very similar protein configurations the transition state and the final state are alike. See below for an explanation of negative $\Delta H^{\neq}$ in this interesting protein system.

Reassuringly, different temperature and viscosity experiments and different theoretical fittings of the apparent rate constant k_{hT}^{tr} gave the same $\Delta G^{\neq}$ values in Table 1 (above 30 °C) and Table 2 (at 40 °C). This consistence supports the notion that the apparent rate constant k_{hT}^{tr} corresponds to rearrangement of the protein complex, a step slower than the electron-transfer step and therefore rate-limiting for the overall process in Eq. (1). We conclude that the reaction within the transient complex above 30 °C occurs by the gated mechanism.

3.7. Coupled electron-transfer reaction, below ca. 30 °C

The H_{AB} value consistent with a nonadiabatic reaction and λ value considerably greater than that expected of a true electron-transfer mechanism, together, are diagnostic of a coupled mechanism [12], which should not be confused with the more common gated mechanism. In the coupled mechanism the apparent rate constant depends not only on the slowest step, which is electron transfer, but also on the preceding rearrangement because this rearrangement, although faster than electron transfer, is thermodynamically unfavorable. But how to distinguish coupled and gated mechanisms? After doubting that solution viscosity can be used for that purpose [11,34,35], we now show that the distinction can reliably be made by careful analysis of viscosity and temperature effects.

Because the apparent rate constant k_{IT}^{tr} depends on viscosity, the process represented by k_{IT}^{tr} involves protein motion. This is one symptom of the coupled mechanism. Now we seek evidence for its defining feature, the unfavorable equilibrium. We justified above the substitution of k^{pr} for k_{et} in Eq. (17). Since both rate constants k_{IT}^{tr} and k^{pr} in Eq. (17) are known from independent experiments, the equilibrium constant is simply obtained with Eq. (18).

$$k_{IT}^{tr} = K_r \times k_{et} = K_r \times k^{pr} \tag{17}$$

$$K_r = \frac{k_{IT}^{tr}}{k^{pr}} = \frac{9\times10^2\ s^{-1}}{1.2\times10^4\ s^{-1}} = (0.08\pm0.04). \tag{18}$$

The value $K_r < 1.0$ agrees with the coupled mechanism [12]. Conversion with Eq. (19) gives $\Delta G_r^0 = 6\pm3$ kJ/mol, the result coming ultimately from the rate constants k_{IT}^{tr} and k^{pr} at a given temperature.

To verify the coupled mechanism, we determined ΔG_r^0 again, differently. We combined Eyring and Marcus theories in the new Eq. (20) and applied this hybrid theory to apparent rate constant k_{IT}^{tr}, which, as Eq. (17) shows, is a product of two factors amenable to these two theories.

$$\Delta G_r^0 = -RT\ln K_r \tag{19}$$

$$k_{IT}^{tr} = \exp\frac{\Delta S_r}{R}\exp\frac{-\Delta H_r}{RT}\times\frac{4\pi^2 H_{AB}}{h(4\pi\lambda RT)^{1/2}}\exp\left[\frac{-\left(\Delta G^0+\lambda\right)^2}{4\lambda RT}\right]. \tag{20}$$

We justifiably fixed the parameters λ and H_{AB} to their true-electron-transfer values in Table 1. Then, fitting temperature dependence of k_{IT}^{tr} to Eq. (20) gave $\Delta H_r = 16\pm3$ kJ/mol and $\Delta S_r = 34\pm8\ J\ K^{-1}\ mol^{-1}$. Small ΔS_r agrees with rapid but thermodynamically unfavorable rearrangement causing a small change in the diprotein configuration. Positive ΔS_r increases the H_{AB} value [11]. Indeed, 4.9 > 0.5 in Table 1. Plugging the values into Eq. (21) gave $\Delta G_r = 6\pm3$ kJ/mol, the result coming ultimately from k_{IT}^{tr} at various temperatures.

$$\Delta G_r = \Delta H_r - T\Delta S_r. \tag{21}$$

The satisfying agreement of the ΔG_r values obtained in two different ways further corroborates our proposition at the beginning of this subsection, that the mechanism is coupled. Since standard Marcus theory does not recognize dynamic factors such as protein rearrangement, coupled mechanism is better treated with our Eq. (20), which recognizes an interplay between rearrangement and electron-transfer steps.

As explained above, $k_{et} = 1\times10^4\ s^{-1}$ for this protein pair. The defining criterion of the coupled mechanism, stated in the Introduction, gives the lower limit $k_r > 1\times10^4\ s^{-1}$ for this diprotein system. The difference between the nominal λ values for the coupled and true reactions in Table 1 is approximately 1.0 eV. Because Marcus theory does not fully apply to coupled reactions, this difference is uncertain. Semiquantitatively, however, this increment of ca. 1.0 eV may be taken as the additional reorganizational energy, beyond that for true electron transfer, required for coupling of the electron-transfer step with protein rearrangement.

3.8. Configurational heterogeneity and energetics of the protein complex

Thorough Brownian dynamics simulations in Fig. 3a show a remarkable "energy seascape" — a nonassociation "sea" surrounding two association "islands" connected by an "isthmus." Two broad ensembles of diprotein configurations appear to be "bridged" by relatively few intermediate configurations. The same qualitative pattern persists at ionic strengths of 10 and 200 mM even though electrostatic interactions are greatly attenuated at the latter value. The color-coded height of this "land" is proportional to the probability of protein association. The right-hand island, containing the tallest mountain, is much more populated, but very long heme–heme distances likely make electron transfer undetectably slow. The left-hand island, featuring two lower hills of

probability, is less populated, but heme–heme distances are favorable for electron transfer. It is reasonable to conclude that the leftmost region of the left-hand island overwhelmingly contributes to the rate constants for rearrangement and electron transfer, as shown in Scheme 1 [5]. In experiments at different viscosities and temperatures (while carefully eliminating viscosity variation *because of* temperature change), we influence the electron-transfer event little or not at all, but we sample the ensembles of protein configurations by the energy required for their rearrangement.

The persistent complex in Scheme 1 is probably relatively homogeneous. A significant fraction of the time-persistent configurations probably are redox-active, either because the initial docking of the two proteins was favorable or, if the initial docking was unfavorable, because these configurations rearrange relatively easily. The protein rearrangements are faster than the electron-transfer step, which therefore becomes rate-limiting. The k^{pr} plots in Fig. 1 show no breaks. We conclude that the persistent complex reacts by true electron-transfer mechanism in the entire interval studied, from 0.5 to 40 °C.

The transient complex in Scheme 1 is more heterogeneous, because the two proteins can collide in various mutual orientations. Indeed, Brownian-dynamics simulations in Fig. 3b show a wide range of heme–heme orientations. To arrive in the short-distance region of the left-hand island in Fig. 3a, the protein pair must undergo a slower rearrangement, requiring more energy. The experiments below ca. 30 °C engage a smaller sample — those configurations that interconvert across lower activation barriers. At these lower temperatures, the electron-transfer mechanism is coupled. Experiments above ca. 30 °C engage a larger sample — those configurations that interconvert across higher barriers. At these higher temperatures, the mechanism is gated. By raising the temperature, we progressively sample more and more configurations in which rearrangement is slower than electron transfer. Now rearrangement becomes the rate-limiting step.

The computational results in Fig. 3a confirm that, as the temperature increases, an increasing number of protein–protein configurations is sampled. An increasing fraction of these newly accessible configurations is redox-inactive, and they must rearrange for electron transfer to occur. This interpretation is consistent with the experimental results in Table 1. Indeed, the entropic contribution to the activation energy is greater above ca. 30 °C than below ca. 30 °C, and the enthalpic contribution is negative above ca. 30 °C. If the average energy of the redox-inactive configurations exceeds the energy of the transition state that must be traversed en route to redox-active configurations, this difference (excess) could give rise to a negative enthalpic contribution to activation energy.

Brownian dynamics simulation reveals the energy landscape required for behavior of this kind. Fig. 3a shows many energetically accessible but redox-inactive configurations and few redox-active ones. As temperature increases, the number of redox-inactive configurations increases, while the number of redox-active ones remains about the same. As the probability of finding redox-active configurations decreases with increasing temperature, the necessary rearrangement into redox-active configurations becomes rate limiting.

Because true and gated mechanisms are clearly different but occur together (above ca. 30 °C) for the same proteins, we can estimate the energetics of gating. We reasonably assume that the rate of the electron-transfer step is governed by activation free energy ($\Delta G^{\neq}$) and not by donor-acceptor coupling (H_{AB}). Knowing $\Delta G^0 = -1.2$ eV and $\lambda = 2.0 \pm 0.2$ eV (an average in Table 1), we calculate $\Delta G^{\neq}$ for the true mechanism to be $(\Delta G^0 + \lambda)^2/4\lambda = 3.2$ k_BT. If so, then $\Delta G^{\neq}$ for the gated mechanism involving cytochrome c_6 and cytochrome *f* must be greater than 3.2 k_BT. Activation free energies for configurational rearrangement of other proteins, and perhaps biomolecules in general, can be estimated along similar lines. Activation free energies cannot be obtained by fittings of kinetic results to available theories, and these energies are useful in analyzing protein dynamics. Our method is an approximate one, but it promises to be a general one.

Association between cyt *f* and cyt c_6 occurs mostly by hydrophobic interactions [11]. Because these interactions are nondirectional, they can hold during the configurational rearrangement, and we implicate them in the energy landscape responsible for the heterogeneous kinetics. That the rates of electron transfer from cyt c_6 to PsaF in the cross-linked and native complexes are identical [36] indicates that cross-linking captures this complex in a redox-active orientation so that rearrangement is not needed. This finding parallels the situation in our cyt c_6/cyt *f* persistent complex. The fact that one of two intracomplex reactions is viscosity-independent means that some of the initial docking configurations in our protein pair are redox-active. Because only about 33% of cyt c_6 cross-linked to the PsaF is able to perform electron transfer [36], a majority of covalently captured configurations in the other protein pair are redox-inactive. These configurations, although favorable for binding, obviously require rearrangement to become reactive.

4. Conclusion

Metalloproteins and other redox proteins associate in multiple binding configurations which are close in energy but only few of which are competent for electron transfer. Depending on the free energy barrier for the interconversion among binding configurations, the oxidoreduction mechanism between the proteins can be true, coupled, gated, or a combination of those. These mechanisms are not semantic niceties but detectable processes. This study suggests that the same overall redox reaction between the same two proteins can occur simultaneously by different mechanisms when multiple binding configurations can interconvert and the energetics is such that configuration ensembles can be sampled by adjusting temperature. Proteins containing not only metal ions but also redox agents such as flavonoids, quinones, and other cofactors might satisfy these energy requirements. Because interfaces among subunits in oligomeric proteins are dynamic, the interwoven mechanisms we found for reactions *between* proteins might occur also *within* redox enzymes such as membrane-bound complexes in respiratory and photosynthetic electron-transport chains.

Cytochrome c_6 and cytochrome *f* are remarkable in two ways: they associate mainly by hydrophobic forces [11], and their oxidoreduction kinetics shows unprecedented heterogeneity. It is tempting to connect these two features. Because hydrophobic interactions are nondirectional, perhaps they allow easy rearrangement, so that the electron transfer between the proteins simultaneously occurs by different mechanisms.

Appendix A. Supplementary data

Supplementary data to this article can be found online at doi:10.1016/j.jinorgbio.2011.09.017.

References

[1] P.B. Crowley, M. Ubbink, Acc. Chem. Res. 36 (2003) 723–730.
[2] G. Kurisu, H. Zhang, J.L. Smith, W.A. Cramer, Science 302 (2003) 1009–1014.
[3] H.B. Gray, J.R. Winkler, Q. Rev. Biophys. 36 (2003) 341–372.
[4] R.C. Lasey, L. Liu, L. Zang, M.Y. Ogawa, Biochemisty 42 (2003) 3904–3910.
[5] Z.X. Liang, I.V. Kurnikov, J.M. Nocek, A.G. Mauk, D.N. Beratan, B.M. Hoffman, J. Am. Chem. Soc. 126 (2004) 2785–2798.
[6] H. Yang, G. Luo, P. Karnchanaphanurach, T.-M. Louie, I. Rech, S. Cova, L. Xun, X.S. Xie, Science 302 (2003) 262–266.
[7] V.L. Davidson, Acc. Chem. Res. 33 (2000) 87–93.
[8] B.M. Hoffman, L.M. Celis, D.A. Cull, A.D. Patel, J.L. Seifert, K.E. Wheeler, J. Wang, J. Yao, I.V. Kurnikov, J.M. Nocek, Proc. Natl. Acad. Sci. U.S.A. 102 (2005) 3564–3569.
[9] E.V. Pletneva, D.B. Fulton, T. Kohzuma, N.M. Kostić, J. Am. Chem. Soc. 122 (2000) 1034–1046.
[10] J.M. Nocek, J.S. Zhou, S.D. Forest, S. Priyadarshy, D.N. Beratan, J.N. Onuchic, B.M. Hoffman, Chem. Rev. 96 (1996) 2459–2489.
[11] T.Ž. Grove, N.M. Kostić, J. Am. Chem. Soc. 125 (2003) 10598–10607.
[12] V.L. Davidson, Biochemistry 39 (2000) 4924–4928.
[13] D. Sun, X. Li, F.S. Mathews, V.L. Davidson, Biochemistry 44 (2005) 7200–7206.

[14] M.M. Crnogorac, C. Shen, S. Young, O. Hansson, N.M. Kostić, Biochemistry 35 (1996) 16465–16474.
[15] Y.-L. Hyun, Z. Zhu, V.L. Davidson, J. Biol. Chem. 274 (1999) 29081–29086.
[16] T.K. Harris, V.L. Davidson, L. Chen, F.S. Mathews, Z.-X. Xia, Biochemistry 33 (1994) 12600–12608.
[17] M.M. Ivković-Jensen, N.M. Kostić, Biochemistry 36 (1997) 8135–8144.
[18] L. Liu, J. Hong, M.Y. Ogawa, J. Am. Chem. Soc. 126 (2004) 50–51.
[19] H. Mei, K. Wang, N. Peffer, G. Weatherly, D.S. Cohen, M. Miller, G. Pielak, B. Durham, F. Millett, Biochemistry 38 (1999) 6846–6854.
[20] H. Anni, J.M. Vanderkooi, L. Mayne, Biochemistry 34 (1995) 5744–5753.
[21] M. Hervas, J.A. Navarro, M.A. De la Rosa, Acc. Chem. Res. 36 (2003) 798–805.
[22] G.M. Soriano, M.V. Ponamarev, R.A. Piskorowski, W.A. Cramer, Biochemistry 37 (1998) 15120–15128.
[23] C.A. Kerfeld, H.P. Anwar, R. Interrante, S. Merchant, T.O. Yeates, J. Mol. Biol. 250 (1995) 627–647.
[24] S. Ye, C. Shen, T.M. Cotton, N.M. Kostić, J. Inorg. Biochem. 65 (1997) 219–226.
[25] S.H. Northrup, K.A. Thomasson, C.M. Miller, P.D. Barker, L.D. Eltis, J.G. Guillemette, A.G. Mauk, S.C. Inglis, Biochemistry 32 (1993) 6613–6623.
[26] J.D. Madura, M.E. Davis, M.K. Gilson, R.C. Wade, B.A. Luty, J.A. McCammon, Rev. Comput. Chem. 5 (1994) 229–267.
[27] G.M. Ullmann, E.-W. Knapp, N.M. Kostić, J. Am. Chem. Soc. 119 (1997) 42–52.
[28] A. Ansari, C.M. Jones, E.R. Henry, J. Hofrichter, W.A. Eaton, Science 256 (1992) 1796–1798.
[29] C. Feng, U. Kappler, G. Tollin, J.H. Enemark, J. Am. Chem. Soc. 125 (2003) 14696–14697.
[30] L. Qin, N.M. Kostić, Biochemistry 33 (1994) 12592–12599.
[31] J.H. Espenson, Chemical Kinetics and Reaction Mechanisms, McGraw-Hill Science, 1995.
[32] R. Frank, G. Greiner, H. Rau, Phys. Chem. Chem. Phys. 1 (1999) 3481–3490.
[33] J.C. Yoder, J.P. Roth, E.M. Gussenhoven, A.S. Larsen, J.M. Mayer, J. Am. Chem. Soc. 125 (2003) 2629–2640.
[34] E.V. Pletneva, M.M. Crnogorac, N.M. Kostić, J. Am. Chem. Soc. 124 (2002) 14342–14354.
[35] L. Qin, N.M. Kostić, Biochemistry 32 (1993) 6073–6080.
[36] M. Hippler, F. Drepper, W. Haehnel, J.-D. Rochaix, Proc. Natl. Acad. Sci. U. S. A. 95 (1998) 7339–7344.